RSC Advances

ROYAL SOCIETY OF CHEMISTRY

www.rsc.org/advances

Journal Name

RSCPublishing

ARTICLE

A Simple Method for Industrialization to Enhance Tap Density of $LiNi_{0.5}Co_{0.2}Mn_{0.3}O_2$ Cathode Material for High-Specific Volumetric Energy Lithium-ion Batteries

Cite this: DOI: 10.1039/x0xx00000x

Received 00th January 2015,
Accepted 00th January 2015

DOI: 10.1039/x0xx00000x

www.rsc.org/

Yin Zhang [a], Zhen-Bo Wang [a,*], Min Nie [b], Fu-Da Yu [a], Yun-Fei Xia [a], Bao-Sheng Liu [a], Yuan Xue [a], Li-Li Zheng [a], Jin Wu [c]

Electrode material with high tap density and high specific volumetric energy is the key of large-scale industrial applications for lithium ion battery industry, which faces huge challenges. $LiNi_{0.5}Co_{0.2}Mn_{0.3}O_2$ cathode materials with different particle sizes are used as the raw materials to study the effect of mass ratio of mixed materials on tap density and electrochemical performance of mixed materials in this work. Physical and electrochemical characterizations demonstrate that the tap density of mixed powders with different particle size is higher than those of materials with single particle size. The tap density of as-prepared material has a trend of decrease with the increase of the ratio of 9 μm particle size in the materials. The highest tap density among all kinds of materials reaches up to 2.66 g cm^{-3}. Besides, the mixed material with mass ratio of 7:2:1 has bigger specific surface area as well as it presents better cycle behaviors and rate capability than other materials. The specific volumetric capacity of this mixed sample reaches up to 394.3 mAh cm^{-3} with 1 C rate charge/discharge, and it has the advance of 8.5 %, 22.2 % and 40.6 % than any single particle size of 9 μm, 6 μm and 3 μm, respectively, which contributes to the industrial production of Li-Ni-Co-Mn-O cathode materials for lithium ion batteries.

1. Introduction

Rechargeable lithium ion battery (LIB) industry is undergoing a rapid expansion in recent years. Because of the superiorities of high voltage, high capacity, long cycle life and safety, LIB has been applied widely not only to small portable electronic devices but also to long-range and large-scale energy storage device, such as Hybrid Electric Vehicle (HEV), Electric Vehicle (EV), civil and military aerospace.[1,2] There are so many researchers who are engaged in improving the performance of both cathode and anode materials.[3,4] However, it seems difficult to achieve a synergy in the process of lots of researches; namely, it is not easy to simultaneously enhance all-round performance of materials effectively. Although a great many modified methods have improved a certain target of materials performance, the results may always be accompanied with a not little sacrifice of other aspects of performance. For instance, some works make efforts to enhance capacity of anode materials via the nano-crystallization technique, but it will bring about negative impacts such as reducing tap density and volume energy density.[5-7] One can imagine that cathode materials will also face the same negative situation using this technique.

It is well known that low tap density, which results in low volume energy density, is one of the key factors in limiting the application and prospects of LIB. Therefore, reducing the level of volume energy density will augment the difficulties for industrialization and commercialization. Then, since many researchers make efforts to improving tap density of anode materials,[8-10] it is indispensable to raise tap density and volumetric specific energy of cathode materials for matching with the anode when they are assembled into full cells.

Many groups do a large amount of researches on enhancing tap density and volumetric specific energy of cathode materials, including spinel,[11,12] olivine[13,14] and layered[15,16] electrodes. $LiCoO_2$ materials are the common electrodes which are widely used in lots of fields at present. However, there are some defects such as high cost and not environment-friendly owing to a lot of cobalt elements that limit application.[17,18] $LiNi_xCo_yMn_{1-x-y}O_2$ (NCM) materials, which were firstly put forward by Ohzuku in 2001,[19] with α-$NaFeO_2$ layered structure have been considered to be the promising cathode materials to replace $LiCoO_2$ for LIB due to their intrinsic characteristics including high capacity, cycling stability, relatively lower cost

and more safety than commercialized $LiCoO_2$ material.[20–24] Among them, $LiNi_{0.5}Co_{0.2}Mn_{0.3}O_2$ (hereafter abbreviated as NCM523) has attracted much attention because of the improvement on specific capacity and the reduction of cost contributed by higher Ni and lower Co contents.[25-27] Some researches focus on improving NCM conductivity in order to enhance rate performance and then to meet the commercial requirement for NCM523.[28-30] But unfortunately, the improving rate performance may cause the decrease of volume energy density.[28] Thus, it still limits the application as mentioned above. To solve this problem, more works focus on the single particles to improve tap density, while their methods are all complicated and difficult to reproduce, resulting in not suitable for large-scale industrial production. For instance, quite a number of researchers devote to the methods of synthesis,[31-35] such as using a co-precipitation method in which all conditions are difficultly controlled simultaneously,[32,34] or a complicated eutectic molten-salt method.[31] And the tap densities obtained by those researches reach the range of 1.72-2.89 g cm^{-3}. Others adopt means of doping bulk phase with Na,[36] B and F,[37] Cr,[38] using co-precipitation method making tap densities arrive the range of 1.71-2.48 g cm^{-3}. Therefore, it is still a challenge to obtain the Ni-based cathode materials with both high electrochemical performance and high tap density using a relative easy way because the electrochemical property, especially rate capability could be improved at the expense of volumetric energy density as mentioned above, which is dependent on the tap density of material.

In short，a high tap density is expected for cathode materials to obtain high volumetric energy density.[39,40] Thus, the volume of batteries could be smaller for the application of commercial lithium ion batteries due to the higher tap density.[36] In this work, we mixed NCM523 cathode materials with different dimensions by certain weight ratios to improve tap density. Meanwhile the commercialized NCM523 with single particle size were used as the contrast sample. The value of specific volumetric capacity was used as the primary factor with consideration to estimate electrochemical properties of all the as-prepared samples for getting higher volumetric energy density compared with present NCM523 material that few references mentioned as we know. Above all, this method in our work can obviously enhance specific volumetric capacity of materials, and is much easier than any other literatures reported in terms of improving tap density and specific volumetric capacity to our knowledge, and it can be replicated easily. As a result, our method is suitable for industrialized production to improve tap density and specific volumetric capacity due to the simple preparation process compared to the literatures report above. And more meaningful is that we believe this method may popularize other spherical or spherical-like electrode materials to meet demand of higher tap density and volume energy density in industrial production.

2. Experimental

2.1 Synthesis of materials

Li_2CO_3 and $Ni_{0.5}Co_{0.2}Mn_{0.3}(OH)_2$ hydroxides (industrial grade, provided by the Xi'an Huijie Industrial CO., LTD.) with different particle sizes were used as the raw materials. And samples mixing with different particle size powders were put into an agate jar with the stoichiometric molar ratio of $Li/(Ni_{0.5}Co_{0.2}Mn_{0.3})(OH)_2$ (1.10:1) to blend anhydrously for half an hour. Then, the uniformly mixing samples were sintered at 850℃ for 12h, following with natural cooling to room temperature according to our previous work.[41,42,43] The synthesized NCM523 materials with particle size of 9 μm, 6 μm and 3 μm were denoted as D9, D6 and D3, respectively. In particular, they were also compared with the mixed materials as the contrast samples.

2.2 Manufacture of electrodes and half cells

Active material, acetylene black as the conductive agent and polyvinylidene fluoride as the blinder with a weight ratio of 8:1:1 were dispersed in appropriate N-methyl-2-pyrrolidone solution and then stirred for 12 h to form slurry. The slurry was coated on an aluminum foil uniformly, and then dried in a vacuum oven under 120 ^oC for 10 h. Subsequently the foil was cut into round slices with 14 mm diameters to be the positive electrode for battery test. Standard CR2025 coin cells were used for electrochemical analysis. Half cells were assembled with pouched slices (positive electrode), polyethylene film (seperator) and Li metal sheet (negative electrode). The electrolyte was 1.0 mol L^{-1} $LiPF_6$ dissolved in ethylene carbonate (EC) and dimethyl carbonate (DMC) (1:1, volume ratio). The concentration of oxygen and humidity in the Ar atmosphere glove box were both well controlled lower than 1.0 ppm at room temperature of 25±0.5 ^oC. Electrochemical measurements were carried out after the fabrication of batteries for the adequate soak of electrolyte and electrode for more than 12 h.

2.3 Characterizations of physical performance

The morphology of samples was performed by a scanning electron microscopy (SEM, SU8000, Hitachi, Japan). Particle distribution was taken with a particle size analyzer (LS 13 320 SW, Bekmam Coulter, U.S.). Surface areas of materials are test by a Surface area analyzer (SSAA, 3H2000, BSD, China). A powder density meter (JZ-7, Jingxin Powder Analyse Instruments Co., Ltd., Chengdu) was used to measure tap density of materials.

2.4 Characterizations of electrochemical properties

Charge-discharge test was performed using a constant current plus constant voltage (CC-CV) mode in a potential range of 3.0-4.3 V with different rates on the Neware battery testing system (Neware Co., Ltd, Shenzhen). Cyclic voltammetry (CV) and electrochemical impendence spectroscope (EIS) measurements were received from a CHI650D electrochemical workstation (CH Instruments, Inc, Shanghai). CV tests took the voltage range from 3.0 to 4.3 V with the sweep speed of 0.1 mV s^{-1}. EIS measurements were performed with the frequent range from 100 kHz to 0.01 Hz in automatic sweep mode from high to low frequencies with the amplitude of 5 mV.

3. Results and discussion

All of the synthesized samples of different particle sizes have good crystallinities with the hexagonal α-$NaFeO_2$ layered structure of an R-3m space group, and there is no impurity peak exists in the XRD patterns as shown in our previous work.[41]

Fig. 1 shows a triangle model of weight ratios of NCM523 materials mixed with different particle sizes (9 μm, 6 μm and 3 μm) for tap density measurements. Tap densities of materials mixed with three kinds of particle sizes in various weight ratios are listed in Table S1.

It can be seen in Table S1 that tap density of materials has an increasing trend with the weight ratio increase of bigger size (D9 and D6) materials, illustrating the fact that the materials with the diameters of 9 μm will mainly contribute to a higher tap density of mixed samples. However, sample 22 which was composed by only small size (D3) material has the lowest tap density of 1.50 g cm^{-3}. Fig. 2 indicates the trends of tap density according to Table S1, changing with different particle sizes.

Fig. 2 shows the curves of tap density changing with different particle sizes of various weight ratios. Fig. 2(a) is the tap density of single samples D9, D6 and D3, respectively. Obviously, tap density decreases with the increasing of particle size, because smaller particles can move to the voids among bigger ones, thus sample D3 does not have enough voids for other particles smaller than itself to move in due to size distributions of the three samples obeying log normal distribution law, which D9 has a wider distribution range than that of D3 according to our previous research.[41] Besides, another reason is that the smaller size the sample has, the more hydroscopicity it performs. Therefore, the powder flowability of D3 is weaker than that of D9. Fig. 2(b), (c) and (d) indicate the influence of tap density by comparing other particle size samples based on a certain proportion of one particle size sample remaining unchanged. Namely, they are contents of D3 or/and D6 in samples with different weight ratios of particle sizes, respectively. And the curves in Fig. 2(b) and (c) indicate that an appropriate mixing of D9 and D6 (or/and D3) will achieve an increase of tap density though D3 will reduce the tap density of mixed samples because of its extremely low tap density (1.50 g cm^{-3}) as shown in Table S1. Though it is not easy to find out that tap density of samples grows up obviously with the increase of percentage of D6 in Fig. 2(d), especially from 10% to 40%, it also can be seen from Table S1 that there is a little rise indeed.

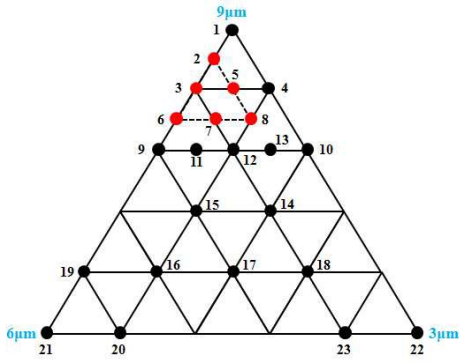

Fig. 1 The triangle model of weight ratios with different particle sizes of NCM523.

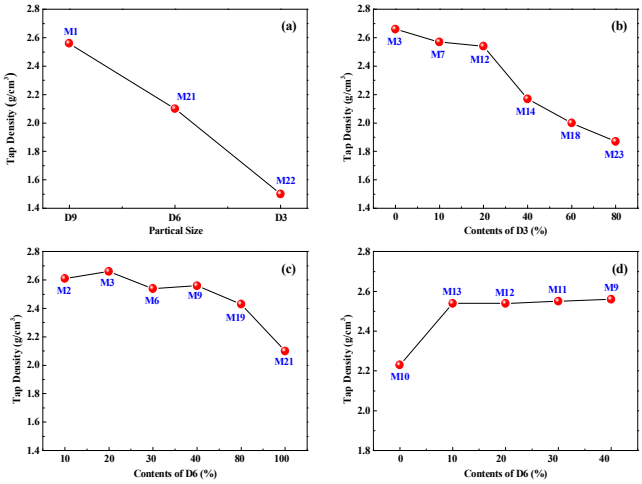

Fig. 2 Curves of tap density *vs*. different of particle sizes with various weight ratios: (a) tap density of single samples D9, D6 and D3; (b) tap density of percentage of D3 in materials with D6 maintaining 20%; (c) tap density of percentage of D6 in materials without D3; (d) tap density of percentage of D6 in materials with D9 maintaining 60%.

To sum up, samples will have a higher tap density as long as mixing a relative smaller size particles into the bigger ones suggested in Fig. 2. However, the materials with lower tap densities could not meet the requirements of industrial production due to the worse volume energy density and lower economic benefit. Therefore, among all the points, we pick out six samples (red points in Fig. 1, where material number of 2, 3, 5, 6, 7 and 8 are named as M2, M3, M5, M6, M7 and M8, respectively) to conduct other characterizations as follows, which have higher tap densities (>2.50 g cm^{-3}), making them an advantage in volume capacity compared with other samples.

The uniformity of mixed samples could be roughly estimated by SEM images, and the morphological characterizations of M6 and M7 samples mentioned above are exhibited in Fig. 3, while SEM images of other samples are shown in Fig. S1. Furthermore, details of particle size distribution parameters are shown in Table S2.

From Fig. 3, it can be believed that the quasi-spherical configuration of material is not destroyed after grind process. Also, materials mixed with different particle sizes are all well-distributed in the view fields of micron scale, meaning that all samples are mixed uniformly by different weight ratios mixing. Fig. 3(a) and (c) are the images of M6, which has the weight ratio of 7:3:0 (D9:D6:D3), while Fig. 3(b) and (d) are the images of M7, which has the weight ratio of 7:2:1 (D9:D6:D3) for comparing. As a result, more interspaces have been taken up by smaller particle size of D3 material, leading to the fact that M7 has a higher tap density than that of M6. BET data are listed in Table 1, and it can also indicate that specific surface area is expanding with the increasing contents of smaller particle size material.

The initial charge-discharge curves of the six samples with rate of 0.2 C are displayed in Fig. 4, and more concerned details are revealed in Table 2. It shows that M7 performs the highest discharge specific capacity of 160.2 mAh g^{-1} with the highest columbic efficiency of 85.3 %, while discharge specific capacities of M8, M2,

M3, M6 and M5 reach to 158.1, 153.5, 151.4, 151.1 and 150.5 mAh g^{-1}, respectively. In addition, the initial charge/discharge capacity has a decrease trend with the increasing contents of D6, in particular, M2, M3 and M6 demonstrate obviously compared with other samples even though the coulombic efficiency is not affected with some great extent.

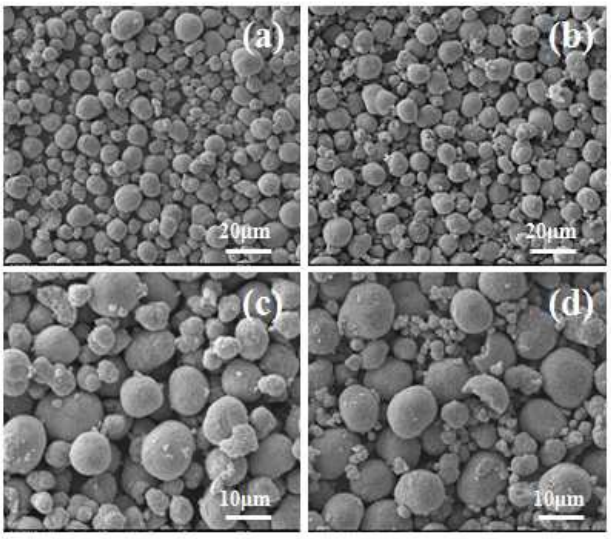

Fig. 3 SEM images and magnifications of mixed NCM523 materials: M6 (a, c) and M7 (b, d).

Table 1 Specific surface area of NCM523 samples with different weight ratios.

Sample	M8	M7	M5	M6	M3	M2
Specific surface area (m^2 g^{-1})	0.3500	0.3277	0.3196	0.2860	0.2639	0.2507

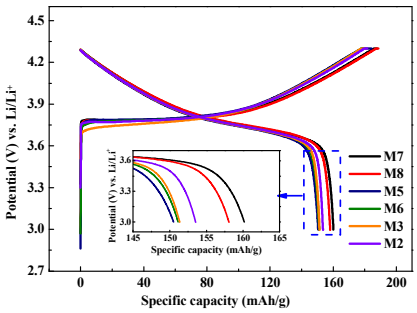

Fig. 4 First cycle charge-discharge (3.0-4.3 V) curves of samples with 0.2 C rate.

Table 2 First cycle charge/discharge and coulombic efficiency of NCM523 materials.

Sample	M7	M8	M2	M3	M6	M5
CC[a] mAh/g	187.8	188.7	181.6	179.6	179.3	184.3
DC[b] mAh/g	160.2	158.1	153.5	151.4	151.1	150.5
CE[c] %	85.3	83.8	84.5	84.3	84.3	81.7

[a] Charge Capacity
[b] Discharge Capacity
[c] Coulombic Efficiency

Fig. 5 shows the cycle behaviors and rate capability of mixed samples, and more relevant details are revealed in Table S3 and Table S4. Fig. 5(a) and (b) show the cyclic curves of both specific gravimetric capacity and specific volumetric capacity of samples, while Fig. 5(c) and (d) perform the rate capability of both specific gravimetric capacity and specific volumetric capacity of samples. It can be seen from Fig. 5(a) that the discharge capacities of samples increase at first and then are steady with a little decrease due to the increasing contents of D9. Therefore, we choose the average capacity of the first 10 cycles to evaluate the performance of mixed samples as follows. Then, the specific volumetric capacity can be calculated from multiplying specific gravimetric capacity by tap density of each sample, and the results are shown in Fig. 5(b). It can be seen that the average specific volumetric capacities of both M7 and M2 for the first 10 cycles at 1 C reach 394.3 mAh cm^{-3} that are higher than those of other samples due to the higher tap densities they have. The average specific volumetric capacities of last 10 cycles for M7 and M2 achieve 379.4 and 370.3 mAh g^{-1}, with the capacity retentions of 96.2 % and 96.4 %, respectively. Fig. 5(c) and (d) show the rate capability of mixed samples, and the charge-discharge process is performed with the same rate between 3.0-4.3 V for each 10 cycles. It demonstrates that M7 has a better rate capability than those of the samples shown in Table S4, and its average volumetric capacities at 1 C, 2 C, 3 C and 5 C reach up to 354.9, 339.7, 325.5 and 314.6 mAh cm^{-3}, respectively, and when it returns to 1 C at last 10 cycles, the capacity returns as well. The capacity retentions (5 C/1 C) of all samples keep over 80%. However, M7 expresses the best rate capability with the retention of 88.7 % for 5 C/1 C. The outstanding rate capability of M7 may be attributed to the more contents of bigger particle size materials like D9 and D6, resulting in the structure stability of material during charge-discharge processes. Furthermore, electrochemistry properties of single size materials (D9, D6 and D3) are compared with the mixed sample M7 as follows, which has the better performance than that of others. Furthermore, the more visual graphical representation is exhibited in Fig. S2.

Electrochemical properties of mixed sample M7 compared with the materials of single particle size (D9, D6 and D3) are shown in Fig. 6. Fig. 6(a) and (b) tell the specific gravimetric and volume capacities of samples while Fig. 6(c) and (d) perform the rate capability of samples. It is obvious that the specific volume capacity of M7 reaches up to 394.3 mAh cm^{-3}, which is much higher than those of single particle size materials due to its high tap density as shown in Fig. 7, even though it has the lower specific gravimetric

capacity. Furthermore, from Fig. 6(b), it can be seen that M7, which is mixed with different particle sizes, has the advance of 8.5 %, 22.2 % and 40.6 % than sample D9, D6 and D3, respectively. Besides, the rate performance of M7 appears better than those of D9, D6 and D3 with capacity retention of 5 C/1 C of 88.1 %, which is higher than those of other samples according to the details shown in Table S5 and Table S6. However, it is unfortunate that the capacity retention of sample M7 is a little worse than that of D9 after 100 cycles as shown in Fig. 6(a) and (b). One of the possible reasons for it might be electrolyte contacting a little hard among bigger size particles, which results in a relatively lower capacity during about the early 10 cycles, and then the capacity rises slowly to a relatively stable status after about 10-20 cycles, because it needs a certain time for the soak between electrolyte and active materials. As a result, the capacity retention of sample D9 is more than 100%. Another reason is that cycling stability of NCM has a bigger fluctuation as the temperature changes, leading to the line type of cycle performance presenting a kind of wave. The temperature is not stable absolutely due to the restriction of testing environment. Even so, the specific volume capacity of M7 is superior to that of single particle size materials.

The reason for the better rate performance of M7 may be the improving speed of electrons and lithium ions transport due to the smaller size materials filling into the interspaces among particles, so that the conductive additive will contact with active materials much more closely than samples with single size particles shown in Fig. 8, which is the SEM of electode cross-section drawn, and the magnifying figure in red frame is shown in lower left quarter of the whole picture. Also, Fig. 8 indicates that there is no significant effect on tap density when they are made into slurry due to its uniformly mixing. Fig. 9 shows the schematic diagram of the path of electrical conduction for both single particle size materials and mixed samples. As it can be seen from Fig. 8 and 9 that single particle size material is more incompact than that of mixed sample,

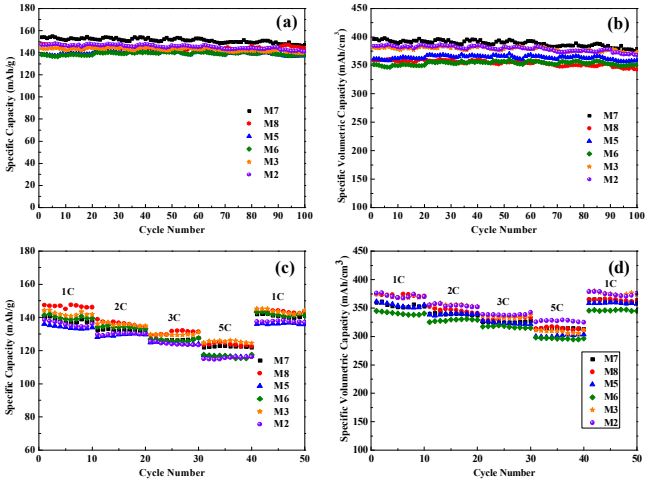

Fig. 5 Electrochemistry properties of mixed samples: (a) specific capacities of mixed samples with the rate of 1 C between the voltage range of 3.0-4.3 V; (b) specific volume capacities of mixed samples according to (a) and their tap densities; (c) specific capacities of mixed samples with different rates between the voltage range of 3.0-4.3 V; (d) specific volume capacities of mixed samples according to (c) and their tap densities

which leads to the invalidation of conductive agent. Thus, that may be one of the reasons why the mixed sample has a better electrochemical performance, especially rate property. As a result, the electrochemical performance of mixed sample is better than any single particle size sample especially for their specific volume capacities, which is one of the most important targets for industrial production. Besides, this method to improve tap density and specific volume capacity is easier and more effective than some other works listed in Table 3, so that it can be used widely in large-scale industrial production.

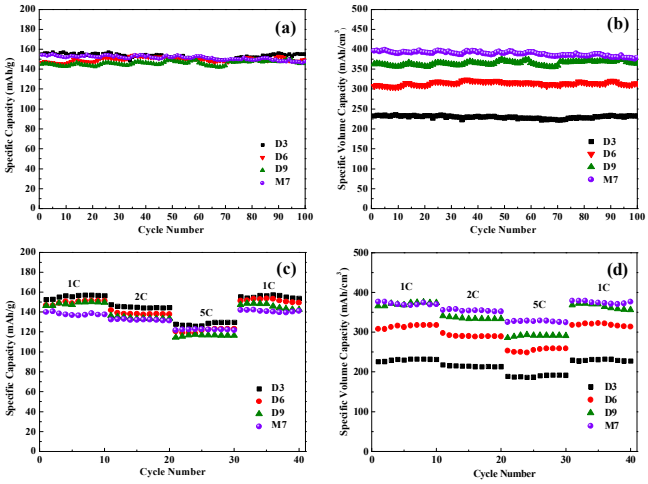

Fig. 6 Electrochemistry properties of M7 compared with singe particle size materials (D9, D6 and D3): (a) specific capacities of samples with the rate of 1 C between the voltage range of 3.0-4.3 V; (b) specific volume capacities of samples according to (a) and their tap densities; (c) specific capacities of samples with different rates between the voltage range of 3.0-4.3 V; (d) specific volume capacities of samples according to (c) and their tap densities.

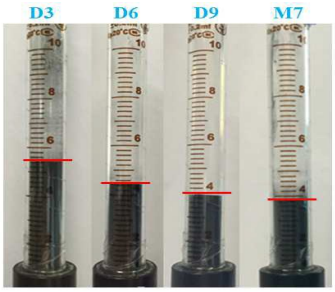

Fig. 7 The picture of tap density text result of different particle size materials.

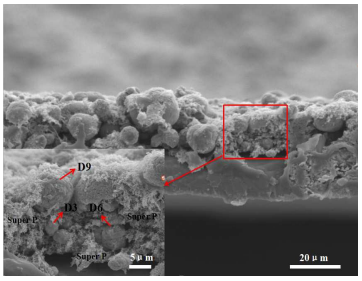

Fig. 8 SEM of electrode cross-section drawn before cycle.

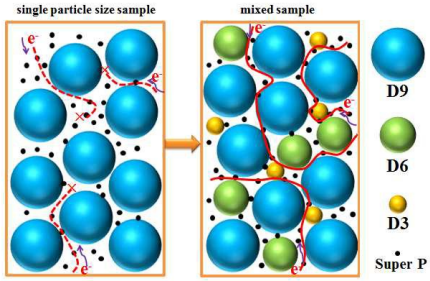

Fig. 9 The schematic diagram of the electrical conduction path for both single particle size materials and mixed samples.

Cyclic voltammetry (CV) measurements of the mixed material M7 compared to D9 are presented in Fig. 10 and the details of other mixed samples are processed in Table S7. It is well known that there are three transition metal elements including Ni, Co, and Mn with different valences of +2, +3 and +4, respectively in NCM cathode material. And Ni^{2+} ions and Co^{3+} ions act as the electrochemical active elements to conduct redox reactions while Mn^{4+} ions remain inert during the process of charge-discharge.[52,53,54] The redox potential of sample can be evaluated from the CV curves. The anodic peaks around 3.8 V within the potential range of 3.0-4.3 V in Fig. 7 for D9 and M7 correspond to the oxidation process of Ni ions from Ni^{2+} to Ni^{3+} and Co ions from Co^{3+} to Co^{4+}, accompanying with the process of Li^+ de-intercalation. The cathodic peak around 3.7 V presents the reverse electrochemical process of Li^+ intercalation. It can be seen from Fig. 10(a) that M7 has a lower potential at the beginning of the peak appearing than that of D9. And the oxidation peak potential of M7 is 3.825 V, which is lower than D9 (3.851 V) due to the bigger specific surface area of M7 for contacting with electrolyte. Besides, all mixed samples have the lower potential at the beginning of the peak appearing compared to D9 as shown in Table S7. However, Fig. 10(b) shows the curves of samples after 100 cycles. Unfortunately, the cycle performance of D9 is better

Table 3 Comparison of other works on researching tap density of different cathode materials with various methods.

Sample	Method	TD[a] (g cm^{-3})	VR[b] (V)	SVC[c] (mAh cm^{-3})	Ref.
$Li[Ni_{1/3}Co_{1/3}Mn_{1/3}]O_2$	hydroxide co-precipitation	2.39	2.8-4.3	380.0 (at 20mAg^{-1})	[44]
$Li[Ni_{1/3}Co_{1/3}Mn_{1/3}]O_2$	hydroxide co-precipitation	2.56	2.8-4.3	426.5 (at 32mAg^{-1})	[45]
$Li[Ni_{1/3}Co_{1/3}Mn_{1/3}]O_2$	two-step drying	2.95	3.0-4.3	492.7 (at 0.2C)	[46]
$Li[Ni_{1/3}Co_{1/3}Mn_{1/3}]O_2$	carbonate co-precipitation	2.19	2.8-4.2	348.2 (at 20mAg^{-1})	[47]
$Li[Ni_{1/3}Co_{1/3}Mn_{1/3}]O_2$	hydroxide co-precipitation	2.38	3.0-4.3	397.4 (at 16mAg^{-1})	[48]
$LiNi_{0.8}Co_{0.15}Mn_{0.05}O_2$	hydroxide co-precipitation	2.72	3.0-4.3	478.7 (at 1C)	[49]
$LiNi_{0.7}Co_{0.15}Mn_{0.15}O_2$	hydroxide co-precipitation	2.37	3.0-4.3	438.9 (at 0.2C)	[50]
$LiNi_{0.6}Co_{0.2}Mn_{0.2}O_2$	hydroxide co-precipitation	2.59	2.8-4.3	445.7 (at 1C)	[51]
$Li[Ni_{1/3}Co_{1/3}Mn_{1/3}]O_2$	eutectic molten-salt	2.89	3.0-4.3	462.4 (at 0.2C)	[31]
$Li[Ni_{0.5}Co_{0.2}Mn_{0.3}]O_2$	hydroxide co-precipitation carbonate co-precipitation	2.68 2.35	3.0-4.3	442.2 (at 0.2C) 364.3 (at 0.2C)	[32]
$Li[Ni_{0.6}Co_{0.2}Mn_{0.2}]O_2$	hydroxide co-precipitation	2.32	2.8-4.3	399.7 (at 1C)	[34]
$Li_{0.97}Na_{0.03}Ni_{0.5}Co_{0.2}Mn_{0.3}O_2$	hydroxide co-precipitation	2.17	3.0-4.6	353.9 (at 1C)	[36]
$Li[(Ni_{1/3}Co_{1/3}Mn_{1/3})_{0.98}Al_{0.02}]O_2$ $Li[(Ni_{1/3}Co_{1/3}Mn_{1/3})_{0.96}Al_{0.02}B_{0.02}]O_{1.98}F_{0.02}$	hydroxide co-precipitation	2.12 2.48	3.0-4.4	332.8 (at 1C) 391.8 (at 1C)	[37]
$LiNi_{0.35}Co_{0.2}Cr_{0.1}Mn_{0.35}O_2$	hydroxide co-precipitation	3.10	2.5-4.5	511.5 (at 20mAg^{-1})	[38]
$Li[Ni_{0.5}Co_{0.2}Mn_{0.3}]O_2$	Simple homogeneous hybrid	2.66	3.0-4.3	394.3 (at 1C)	our work

[a] Tap Density
[b] Voltage Range
[c] Specific Volumetric Capacity (calculated by author according to TD and VR)

than M7 after 100 cycles according to the decrease of their peak potential differences ($\triangle E$). However, the result conforms to the capacity of D9, which the capacity retention is more than 100 % after charge-discharge process for 100 cycles in Fig. 6(a) and Table S5 by reason of hard electrolyte contacting among bigger size particles. In spite of this, the better performance of mixed samples could remedy the deficiency of single particle size materials especially for industrial production. Moreover, the rate property is also good, informed by electrochemical impedance spectroscopy (EIS) data.

Fig. 11 shows the electrochemical impedance spectroscopy (EIS) curves of mixed material M7 and single size sample D9 before charge-discharge process, and the parameters of equivalent circuit for them are listed in Table 4. It can be seen from Fig. 11(a) that the curves are all consisted of three semicircles and an oblique line at high, medium-high, intermediate and low frequency, respectively. The intercept on real axis and the first semicircle stands for the ohmic resistance (R_s) and resistance of lithium ions diffusion through the solid electrolyte interphase film (R_{sei}). The second semicircle represents the interface electronic resistance (R_e) of active materials, while the third semicircle represents the charge transfer resistance (R_{ct}), which is the important message to investigate electrochemical performance, especially the rate property of materials. In addition, the oblique line at low frequency is the impedance for lithium-ion diffusion inside material bulk.[55,56,57] Fig. 11 and Table 4 illustrate that M7 owns a smaller value of Rct (7.513Ω) than that of D9 (15.12Ω), which is the reason for its better rate performance. Fig. 11(b) shows the relationships between Z' and $\omega^{-1/2}$ of sample D9 and M7. Here, ω is angular frequency, which can be obtained by the equation (1). Furthermore, Li-ion diffusion coefficient of materials can be obtained according to the formula (2) as shown below.[58]

$$\omega=2\pi f \qquad (1)$$

$$D_{Li}^{+}=\frac{R^2T^2}{2A^2n^4F^4C^2\sigma^2} \qquad (2)$$

In this equation, there are fore constants of R, T, n and F that represent gas constant, temperature, number of electrons in reaction and Faraday constant, respectively. Meanwhile, the surface area (A) and the concentration of Li^+ (C) are of no difference in the same system. Therefore, the Warburg coefficient (σ), which is the slope in Fig. 11(b) mentioned above, becomes the only factor to affect the value of D_{Li}^{+}. Also, it can be seen from formula (2) that D_{Li}^{+} has negative correlation with σ, namely, the bigger slope it shows, the smaller D_{Li}^{+} the sample has, and vice versa. Hence, it is shown in Fig. 11(b) that the slope value of M7 is 3.79293, which is smaller than that of D9, leading to the bigger D_{Li}^{+} of M7 than that of D9. As a result, it can also illustrate why sample M7 has a better rate performance than that of D9, which is agreed with Fig. 6(d).

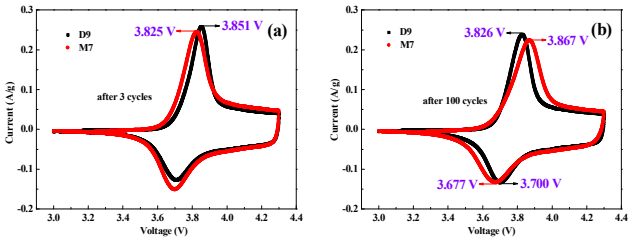

Fig. 10 Cyclic voltammetry curves of M7 compared with D9 before and after cycles, (a) is CV curves after 3 activation process with low current rate of 0.1 C from 3.0-4.3 V; (b) is CV curves after 100 cycles with the rate of 1 C from 3.0-4.3 V.

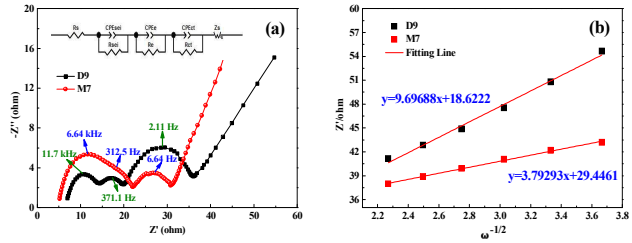

Fig. 11 EIS curves of D9 and M7 before charge-discharge process, (a) Nyquist plots of D9 and M7; (b) the relationships between Z' and $\omega^{-1/2}$ of D9 and M7.

Table 4 Parameters of equivalent circuit for D9 and M7 before charge-discharge process.

Sample	R_s (Ω)	R_{sei} (Ω)	R_e (Ω)	R_{ct} (Ω)
D9	6.767	6.959	6.434	15.12
M7	5.152	8.878	8.278	7.513

4. Conclusion

Layered NCM523 materials were prepared by precursors with different particle sizes of 9μm，6μm and 3μm. All samples with different weight ratios of D9, D6 and D3 are mixed uniformly with the typical α-$NaFeO_2$ layered structure. Among all the samples mixed, M7 with the weight ratio of 7:2:1 (D9:D6:D3) has a comparatively high tap density of 2.57 g cm^{-3} and the highest specific volume capacity of 394.3 mAh cm^{-3}, and it has the advance of 8.5 %, 22.2 % and 40.6 % than any single particle size of 9 μm, 6 μm and 3 μm, respectively In addition, it has the better rate performance than any single size samples. The method of mixing different size particles can obviously enhance tap density and specific volume capacity of materials. Further more, long cycle performance of layered cathode materials would be researched in the later work. But above all, the method is easier than any other research reported to our knowledge in improving tap density or volume capacity, so that it is suitable for widely industrialized production. We also believe that the method may popularize other spherical or spherical-like electrode materials to enhance tap

density, and the works on improving tap density of other cathode materials in order to meet demand of industrial production is the future research direction of our group.

Acknowledgment

We acknowledge the National Natural Science Foundation of China (Grant No. 21273058), China postdoctoral science foundation (Grant No.2012M520731 and 2014T70350), Heilongjiang postdoctoral financial assistance (LBH-Z12089) for their financial support.

Notes and references

[a] MIIT Key Laboratory of Critical Materials Technology for New Energy Conversion and Storage, School of Chemistry and Chemical Engineering, Harbin Institute of Technology, No.92 West-Da Zhi Street, Harbin, 150001 China. E-mail: wangzhb@hit.edu.cn; Tel.: +86-451-86417853; Fax: +86-451-86418616

[b] College of chemical and chemical engineering, Harbin Normal University, Harbin Heilongjiang 150025, China

[c] Xi'an Huijie Industrial Co., Ltd., Xi'an, 710116 China

† Electronic Supplementary Information (ESI) available: [details of any supplementary information available should be included here]. See DOI: 10.1039/b000000x/

1. B. Scrosati, J. Hassounab and Y. K. Sun, *Energy Environ. Sci.*, 2011, **4**, 3287-3295.
2. J. B. Goodenough and K. S. Park, *J. Am. Chem. Soc.*, 2013, **135** (4), 1167-1176.
3. A. Manthiram, J. C. Knight, S. T. Myung, S. M. Oh and Y. K. Sun, *Adv. Energy Mater*. 2016, **6**, 1501010.
4. Z. Y. Wang, L. Zhou and X. W. Lou, *Adv. Mater.*, 2012, **24**, 1903-1911.
5. M. Gauthier, D. Mazouzi, D. Reyter, B. Lestriez, P. Moreau, D. Guyomard and L. Rou´e, *Energy Environ. Sci.*, 2013, **6**, 2145-2155.
6. J. Liu, Q. Zhang, Z. Y. Wu, J. T. Li, L. Huang and S. G. Sun, *ChemElectroChem*, 2015, **2**, 611-616.
7. D. C. Lin, Z. D. Lu, P. C. Hsu, H. R. Lee, N. Liu, J. Zhao, H. T. Wang, C. Liu and Y. Cui, *Energy Environ. Sci.,* 2015, **8**, 2371-2376.
8. H. G. Jung, S. T. Myung, C. S. Yoon, S. B. Son, K. H. Oh, K. Amine, B. Scrosati and Y. K. Sun, *Energy Environ. Sci.*, 2011, **4**, 1345-1351.
9. V. Etacheri, G. A. Seisenbaeva, J. Caruthers, G. Daniel, V. Etacheri, G. A. Seisenbaeva, J. Caruthers and G. Daniel, *Adv. Energy Mater.*, 2015, **5**, 1401289.
10. K. C. Klavetter, P. Souza, A. Heller and C. Buddie Mullins, *J. Mater. Chem. A*, 2015, **3**, 5829-5834.
11. H. Zhang, Y. L. Xu and D. Liu, *RSC Adv.*, 2015, **5**, 11091-11095.
12. J. C. Fang, Y. F. Xu, G. L. Xu, S. Y. Shen, J. T. Li, L. Huang and S. G. Sun, *J. Power Sources*, 2016, **304**, 15-23.
13. C. W. Sun, S. Rajasekhara, J. B. Goodenough and F. Zhou, *J. Am. Chem. Soc.*, 2011, **133**, 2132-2135.
14. X. M. Lou and Y. X. Zhang, *J. Mater. Chem.*, 2011, **21**, 4156-4160.
15. J. M. Zheng, X. B. Wu and Y. Yang, *Electrochim. Acta*, 2011, **56**, 3071-3078.
16. H. J. Kim, H. G. Jung, B. Scrosati and Y. K. Sun, *J. Power Sources*, 2012, **203**, 115-120.
17. S. T. Myung, S. Komaba, K. Hosoya, N. Hirosaki, Y. Miura and N. Kumagai, *Chem. Mater.*, 2005, **17**, 2427-2435.
18. Q.Q. Jiang, L. Xu, J. Huo, H. Zhang and S. Y. Wang, *RSC Adv.*, 2015, **5**, 75145-75148.
19. T. Ohzuku and Y. Makimura, *J. Chem. Lett.*, 2001, **30**, 642-643.
20. N. Yabuuchi and T. Ohzuku, *J. Power Sources*, 2003, **119-121**, 171-174.
21. T. Mei, Y. C. Zhu, K. B. Tang and Y. T. Qian, *RSC Adv.*, 2012, **2**, 12886-12891.
22. Y. Wang, H. Zhang, W. H. Chen, Z. Y. Ma and Z. C. Li, *RSC Adv.*, 2014, **4**, 37148-37156.
23. X. Zhao, Q. C. Zhuang, C. Wu, K. Wu, J. M. Xu, M. Y. Zhang and X. L. Sun, *J. Electrochem. Soc.*, 2015, **162** (14) A2770-A2779.
24. D. Kim, J. M. Lim, Y. G. Lim, J. S. Yu, M. S. Park, M. Cho and K. Cho, *Chem. Mater.*, 2015, **27**, 6450-6456.
25. T. Liu, S. X. Zhao, K. Z. Wang, C. W. Nan, *Electrochim. Acta*, 2012, **85**, 605-611.
26. J. Shu, R. Ma, L. Y. Shao, M. Shui, K. Q. Wu, M. M. Lao, D. J. Wang, N. B. Long and Y. L. Ren, *J. Power Sources*, 2014, **245**, 7-18.
27. P. Y. Hou, X. Q. Wang, D. G. Wang, D. W. Song, X. X. Shi, L. Q. Zhang, J. Guo and J. Zhang, *RSC Adv.*, 2014, **4**, 15923-15929.
28. F. X. Wang, S. Y. Xiao, Z. Chang, Y. Q. Yang and Y. P. Wu, *Chem. Commun.*, 2013, **49**, 9209-9211.
29. Z. D. Huang, X. M. Liu, S. W. Oh, B. Zhang, P. C. Ma and J. K. Kim, *J. Mater. Chem.*, 2011, **21**, 10777-10784.
30. Z. H. Yang, J. B. Lu, D. C. Bian, W. X. Zhang, X. N. Yang, J. F. Xia, G. D. Chen, H. Y. Gu and G. Ma, *J. Power Sources*, 2014, **272**, 144-151.
31. Z. R. Chang, Z. J. Chen, F. Wu, H. W. Tang, Z. H. Zhu, X. Z. Yuan and H. J. Wang, *Solid State Ionics*, 2008, **179**, 2274-2277.
32. S. Y. Yang, X. Y. Wang, X. K. Yang, Z. L. Liu, Y. S. Bai, Y. P. Wang and H. B. Shu, *J. Solid State Electrochem.*, 2012, **16**, 2823-2836.
33. K. C. Wu, F. Wang, L. L. Gao, M. R. Li, L. L. Xiao, L. T. Zhao, S. J. Hu, X. J. Wang, Z. L. Xu and Q. G. Wu, *Electrochim. Acta*, 2012, **75**, 393-398.
34. L. W. Liang, K. Du, W. Lu, Z. D. Peng, Y. B. Cao and G. R. Hu, *Electrochim. Acta*, 2014, **146**, 207-217.
35. Y. T. Zhang, P. Y. Hou, E. L. Zhou, X. X. Shi, X. Q. Wang, D. W. Song, J. Guo and L. Q. Zhang, *J. Power Sources*, 2015, **292**, 58-65.
36. W. B. Hua, J. B. Zhang, Z. Zheng, W. Y. Liu, X. H. Peng, X. D. Guo, B. H. Zhong, Y. J. Wang and X. L. Wang, *Dalton Trans.*, 2014, **43**, 14824-14832.
37. S. Y. Ye, Y. Y. Xia, P. W. Zhang and Z. Y. Qiao, *J. Solid State Electrochem.*, 2007, **11**, 805-810.
38. Y. C. Sun, Y. G. Xia and H. Noguchi, *J. Power Sources*, 2006, **159**, 1377-1382.
39. Y. Kim and D. Kim, *ACS Appl. Mater. Interfaces*, 2012, **4**, 586-589.
40. H. G. Jung, S. T. Myung, C. S. Yoon, S. B. Son, K. H. Oh, K. Amine, B. Scrosati and Y. K. Sun, *Energy Environ. Sci.*, 2011, **4**, 1345-1351.
41. M. Nie, Y. F. Xia, Z. B. Wang, F. D. Yu, Y. Zhang, J. Wu and B. Wu, *Ceram. Int.*, 2015, **41**, 15185-15192.
42. Y. F. Xia, M. Nie, Z. B. Wang, F. D. Yu, Y. Zhang, L. L. Zheng, J. Wu and K. Ke, *Ceram. Int.*, 2015, **41**, 11815-11823.
43. Y. Zhang, Z. B. Wang, J. Lei, F. F. Li, J. Wu, X. G. Zhang, F. D. Yu and K. Ke, *Ceram. Int.*, 2015, **41**, 9069-9077.
44. M. H. Lee, Y. J. Kang, S. T. Myung, Y. K. Sun, *Electrochim. Acta*, 2004, **50**, 939-948.
45. S. Zhang, *Electrochim. Acta*, 2007, **52**, 7337-7342.

46. Z. R. Chang, Z. J. Chen, F. Wu, H. W. Tang, Z. H. Zhu, X. Z. Yuan and H. J. Wang, *Electrochim. Acta*, 2008, **53**, 5927-5933.
47. P. He, H. R. Wang, L. Qi and T. Osaka, *J. Power Sources*, 2006, **160**, 627-632.
48. X. F. Luo, X. Y. Wang, L. Liao, S. Gamboa and P. J. Sebastian, *J. Power Sources*, 2006, **158**, 654-658.
49. K. K. Cheralathan, N. Y. Kang, H. S. Park, Y. J. Lee, W. C. Choi, Y. S. Ko, Y. K. Park, *J. Power Sources*, 2010, **195**, 1486-1494.
50. Z. G. Lu, X. X. Tan, Y. G. Tang and K. C. Zhou, *Rare Met.*, 2014, **33** (5), 608-614.
51. L. W. Liang, K. Du, Z. D. Peng, Y. B. Cao, J. G. Duan, J. B. Jiang and G. R. Hu, *Electrochim. Acta*, 2014, **130**, 82-89.
52. T. L. Zhao, S. Chen, L. Li, X. F. Zhang, R. J. Chen, I. Belharouak, F. Wu and K. Amine, *J. Power Sources*, 2013, **228**, 206-213.
53. Y. Koyama, I. Tanaka, H. Adachi, Y. Makimura and T. Ohzuku, *J. Power Sources*, 2003, **119**, 644-648.
54. S. N. Nikkan and N. Munichandraiah, *ACS App. Mater. Interfaces*, 2009, **1**, 1241-1249.
55. D. W. Abarbanel, K. J. Nelson and J. R. Dahn, *J. Electrochem. Soc.*, 2016, **163** (3), A522-A529.
56. L. Wang, J. S. Zhao, X. M. He, J. Gao, J. J. Li, C. R. Wan and C. Y. Jiang, *Int. J. Electrochem. Sci.*, 2012, **7**, 345-353.
57. X. Y. Qiu, Q. C. Zhuang, Q. Q. Zhang, R. Cao, Y. H. Qiang, P. Z. Ying and S. G. Sun, *J. Electroanal. Chem.*, 2013, **688**, 393-402.
58. L. J. Li, Z. Y. Chen, Q. B. Zhang, M. Xu, X. Zhou, H. L. Zhu and K. L. Zhang, *J. Mater. Chem. A*, 2015, **3**, 894-904.